BOR DERGİSİ
JOURNAL OF BORON
Journal homepage: www.journal.boren.gov.tr

Characterization of W_2B nanocrystals synthesized by mechanochemical method

Mustafa Barış[1], Tuncay Şimşek[2], Hakan Gökmeşe[3], Adnan Akkurt[4]

[1]Eti Mine Works General Management, 06105 Ankara, Turkey

[2]Hacettepe University, Department of Physics Engineering, 06800 Ankara, Turkey

[3]Necmettin Erbakan University, Department of Metallurgical and Materials Engineering, 42090 Konya, Turkey

[4]Gazi University, Department of Industrial Design Engineering, 06500 Ankara, Turkey

ARTICLE INFO

Artlice history:
Received 6 February 2016
Received in revised form 21 March 2016
Accepted 21 March 2016
Available online 24 March 2016

Keywords:
Ball milling,
mechanochemical synthesis,
nanocrystals,
W_2B.

ABSTRACT

In this study; W_2B nanocrystals were synthesized with B_2O_3/Mg/WO_3 starting materials via mechanochemical method. Starting materials were mixed according to the reaction stoichiometry and reduction processes were performed in a planetary ball mill under Argon gas atmosphere. Phase and morphology structure of particles were characterized by X-ray diffraction (XRD), scanning electron microscopy (SEM), transmission electron microscopy with energy-dispersive X-ray spectroscopy (TEM/EDX) and the specific surface area was measured by Brunauer-Emmet-Teller (BET) theory. The effect of milling period and molar ratios of starting powders were investigated in detail. Results showed that W_2B nanocrystals were obtained successfully without different tungsten compounds after 30 h milling and purification in 2 M HCl solution. Coaxial/spherical shaped and agglomerated W_2B nanocrystals were observed by microstructural examinations. Crystallite size and specific surface area of the W_2B nanocrystals were determined as 13.61 nm and 18 m^2/g respectively.

1. Introduction

Tungsten boride compounds (W_2B, WB, W_2B_5, WB_4 and WB_{12}) have remarkable properties like high hardness, melting point and electrical resistivity [1]. There are many methods for production of tungsten borides such as chemical vapour deposition, solid state reaction, ionic melts, self-propagating high temperature synthesis, arc plasma melting and mechanochemical method. Syntheses of these compounds are started in 1960's by Woods et al. and by Peshev et al. [2-3]. In the following years, some properties like mechanical and electrical properties were investigated by some researchers [4-6]. Itoh et al. synthesized W_2B, WB, W_2B_5 and WB_4 compounds via thermal method with elemental tungsten and amorphous boron powders in 1987 [7]. The contribution of W_2B_5 to oxidation resistance of composite materials was investigated by Radev et al. in 1993 [8]. In 1995, Otani et al. produced a WB_{2-x} single crystal via melting process and studied the effects of the boron on the crystal structure [9]. In the same year by melting method Okada et al. produced W_2B, δ-WB and WB_2 crystals and determined the hardness, electrical conductivity and oxidation resistance properties of crystals [10]. Gostishchev et al. have produced W-W_2B and W-WB powders via the reduction of metal oxides and boron mixtures with magnesium in molten salts and demonstrated the effect of NaF-NaCl systems on phases of final product [11]. Mohammadi et al. have produced WB_4 via elements in arc furnace melting method in 2011 [12]. Yeh et al. [13] and Yazıcı et al. [14-15] have produced and characterized a tungsten boride compound via self-propagating high-temperature synthesis (SHS) using oxides form of tungsten. Besides studies for synthesizing and characterization of tungsten boride compounds, coating [16-17] and composite material development studies [18-19] have also been carried out in the literature. Studies for determining the physical and chemical properties of the synthesized compounds of tungsten boride are expected to lead to an increase in practical work in the future [20-24].

*Corresponding author: mustafabaris@etimaden.gov.tr

A number of studies have been reported for transition metal boride via mechanochemical method in the literature [25-41], but there are only a few studies for production of tungsten boride [42-44]. In one of these studies, Coskun et al. have reduced tungsten oxide and boron oxide with Mg and leached the obtained powder mixture with HCl and produced W_2B_5. [42]. Tabrizi and et al. investigated the effect of boron amount on the tungsten boride phases which were synthesized by mechanochemical method [43]. Bahrami-Karkevandi et al. investigated the phase changes of WO_3-B_2O_3-Mg ternary system according to milling period. It is reported that the formation of W_2B-W nanocomposite powders after 60 min of milling was achieved [44].

To the best of our knowledge, it is noticed that W_2B phases were not obtained alone via mechanochemical method. In the most of studies, it was seen that synthesized W_2B powders were composed of different W_xB_y phases [42-44]. In this study, W_2B nanocrystals were synthesized without any other phases of tungsten or tungsten boride via mechanochemical method by changing reaction stoichiometry. The W_2B nanocrystals synthesizing route, morphology and characterization were discussed in detail.

2. Materials and method

2.1. Materials

As starting materials, B_2O_3 (Eti Maden, 545.74 µm, 98.00 %), Mg (Aldrich, 138.66 µm, 99.00 %) and WO_3 (Merck, 3.03 µm, 99.50 %) were used. All experiments were performed under Argon gas atmosphere in a hardened steel vial and 3x15 mm hardened steel balls. 2 M HCl (aq) solution was used for purification of powder mixtures.

2.2. Mechanochemical synthesis method and characterization

The milling processes were carried out by planetary high energy ball mill (Fritsch P6). The synthesis studies were performed with different reaction stoichiometry. In the all experiments, Mg was used 20% wt excess for the reduction reactions and possible oxygen remained in the vial. In the first stoichiometry, B_2O_3's molar ratio was not changed while its molar ratio increased twice in the second stoichiometry. Mixtures of starting materials were prepared according to Equation 1 and placed with balls into vial and sealed tightly in the glove box. At the first stage of milling, WO_3 and B_2O_3 were reduced by Mg (Eq. 1.1 & 1.2 and so on). During the milling, MgO phase was occurred while W and B were released in the vial. Then, W and B reacted by the effect of mechanical energy and formed a W_2B ceramic phase (1.3).

$$4WO_3 + B_2O_3 + 15Mg \longrightarrow 2W_2B + 15MgO \qquad (1)$$

$$4\,WO_3 + 12Mg \longrightarrow 4W + 12MgO \qquad (1.1)$$

$$B_2O_3 + 3\,Mg \longrightarrow 2B + 3MgO \qquad (1.2)$$

$$4W + 2B \longrightarrow 2W_2B \qquad (1.3)$$

Starting powders prepared at 4:1:18 and 4:2:18 molar ratios were milled according the parameters given in Table 1. Then mixtures were milled up to 30 h and analyzed by XRD in every 5 h periods. The powders obtained after milling were purified via aqueous HCl solution prepared with distilled water. Leaching process was performed by using 2 M HCl solution at 400 rpm for 30 minutes at room temperature and 1 g/250 ml were used as a solid to liquid ratio. After leaching, particles were firstly washed with distilled water-ethanol and dried in a vacuum oven at 70 °C for 12 h.

Table 1. Experimental conditions of W_2B nanocrystals

Total Powder Mass (g)	Vial Capacity (mL)	Ball diameter (mm)	Number of balls	Ball to powder ratio (BPR)	Rotation speed (rpm)	Time (h)
1,4	80	15	3	30:1	350	5 10 20 30

Phase structure was determined by X-Ray Diffraction Pattern (XRD, Rigaku, D/MAX-2200, Cu–Kα radiation, 4°/min, 2θ:2-90°, 40 kV, 30 mA). Particle morphologies and microstructures were examined by Scanning Electron Microscope (SEM, FEI, Quanta 200F) and high-definition Transmission Electron Microscope (HRTEM, FEI, Tecnai G2 F30). The specific surface area was measured by Brunauer-Emmet-Teller (BET) apparatus (Quantachrome, Nova 2200E, UK) through nitrogen adsorption/desorption.

Crystallite sizes of the powders were calculated by using the Scherrer formula in Eq. 2.

$$\tau = \frac{K \cdot \lambda}{\beta \cdot \cos\theta} \qquad (2)$$

In the formula; τ is the crystallite size, *K* is the constant taken according to the crystal shape (0,89), λ is the X-ray wavelength (0,154 nm), β is the full width at half maximum (FWHM) and θ is the Bragg angle. Crystallite size calculations were performed according to (100) peak of WB_2 and the FWHM values used were specified in the graphical analysis made in XRD analysis software JADE 7.0.

3. Results and discussion

Figure 1 shows the SEM image and XRD pattern of the unmilled powders. From the SEM image, it was observed that WO_3 and B_2O_3 were in irregular powder shape and morphology while Mg was in flat/flaky morphology. Crystalline WO_3 (PDF-032-1395) and Mg (PDF-01-089-4244) were observed in the XRD pattern, but B_2O_3 was not observed because of its amorphous structure.

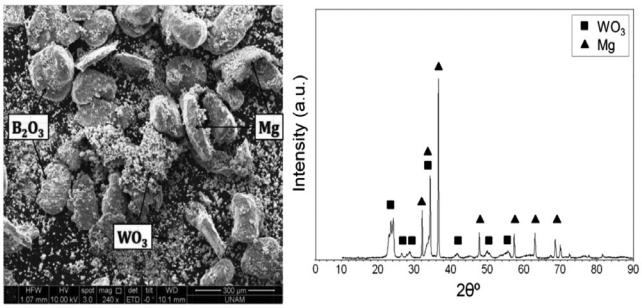

Figure 1. SEM image and XRD pattern of initial powders

Starting powders were prepared at 4:1:18 and 4:2:18 molar ratios. Firstly, powder mixture with 4:1:18 molar ratio was ball milled up to 30 h. XRD pattern of the milled powder is presented in Figure 2. As can be seen from this figure, milled powder mixture was composed of W (peaks at about 2θ ~ 40.267º, 58.260º, 73.196º), W_2B (22.565º, 32.125º, 37.900º, 40.898º, 46.070º, 51.886º, 67.197º, 72.749º, 85.424º) and MgO (36.889º, 42.856º, 62.216º, 74.577º) phases and some Fe (44.673º, 65.022º, 82.334º) contamination was seen in the synthesized powders because of worn of vial and balls. Similar situation was also reported in the Bahrami-Karkevandi's et al. studies. It was reported that powder mixture was composed of W, WB, W_2B and MgO phases via milling [44]. Existing of W phase and transition between phases in the final mixture was probably because of absence of B amount in the reaction environment. Therefore, the molar ratio of B was increased twice in the second stoichiometry for this study.

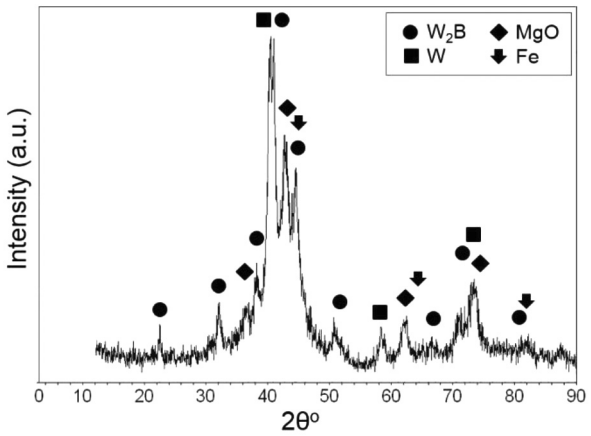

Figure 2. XRD pattern of milling up to 30 h with powder mixture prepared at 4:1:18 molar ratio

Figure 3 shows the XRD pattern of milled powder mixtures prepared at 4:2:18 molar ratio at selected times (1, 10, 20 and 30 h). It was observed from the figure that the diffraction peaks were shortened and the areas under peaks were expanded over the milling. This phenomena explained by the grain size and crystallite size of starting powders decreasing via plastic deformation inflicted by compressive force of ball-powder-ball collisions [41]. As seen from the XRD pattern, the grain sizes of initial powders were decreased at the end of the first hour of milling. After 10 h milling, W (peaks at about 2θ ~ 40.267º, 58.260º, 73.196º), WB (29.961º, 36.191º, 42.194º, 52.715º), W_2B (22.565º, 32.125º, 37.900º, 40.898º, 46.070º, 51.886º, 67.197º, 72.749º, 85.424º), MgO (36.889º, 42.856º, 62.216º, 74.577º) phases were observed in the powder mixtures. But there was also Fe (44.673º, 65.022º, 82.334º) contamination caused by worn of hardened steel vial and balls. With milling up to 20 h, the height of peaks of W and WB were decreased and the peaks of impurities were nearly disappeared. Prolonging the milling time to 30 h, the only phase of W_2B and MgO were observed.

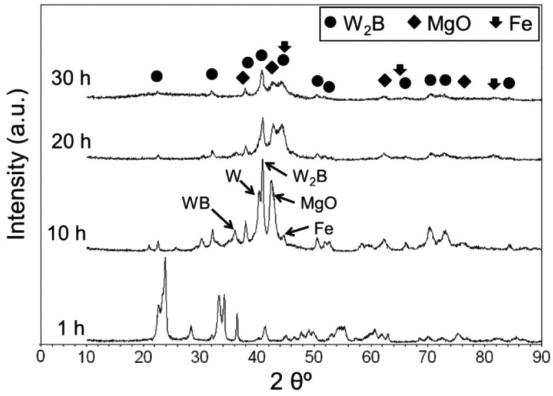

Figure 3. XRD pattern of milling up to 30 h powder mixture prepared at 4:2:18 molar ratio

In the mechanochemical method, mechanism such as flattening, cold welding, fraction, and re-flattening of starting powders occurs by mechanical energy released during the milling. This repeated mechanism causes the decrease in the grain size while it increases the surface area of the particles. Therefore, increased surface area improves the chemical reactivity of the powders. Figure 4 shows the 5 h milled particles images taken by SEM. Fracturing, flattening and cold welding mechanism occurred by the mechanochemical method can be seen clearly in these images. Particles are firstly fractured and cold welded, then agglomerated and formed a coarse particle.

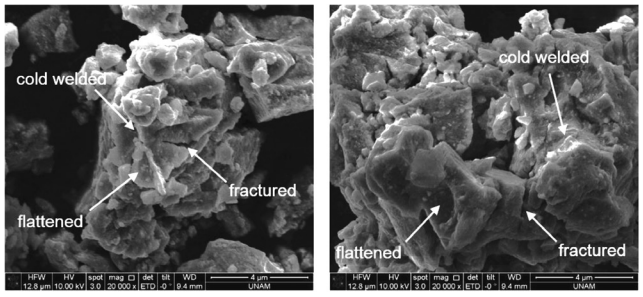

Figure 4. SEM images of the powders milled up to 5 h

In addition, Figure 5 also shows the SEM images of the powder mixtures milled at 1, 10 and 30 h. When the SEM images are examined, due to the formation

of agglomeration, it was observed that similar microstructures were seen in terms of the time variables. It can be considered from the figure that powders at the beginning of synthesis, transformed from ductile-ductile structure to ductile-brittle structure. Powder particles were flattened over time so that after repeated of this mechanism particle sizes were decreased significantly. It was determined that shapes of the particles were mostly in nearly coaxial/spherical shape and morphology towards to end of rnilling. After 1 h grinding, aggregate size of about 50 µm (a) were observed from the SEM images given in Figure 5. With the progress of grinding to 10 h (b) and 30 h (c), aggregate size ranges were decreased to approximately under ~5 µm and ~2 µm, respectively. It was also seen from the SEM images that wide ranges of initial particle size distribution at the beginning of grinding were decreased sharply with prolonged grinding period.

XRD patterns of final powder mixtures before and after purifying processes were given in Figure 6. The figure indicates that the powder mixtures were composed of W_2B, MgO and Fe phases after mechanochemical synthesis. By purification, MgO and Fe were eliminated and final compound was composed of W_2B phase without other tungsten boride phases. Furthermore, because of excess usage of Mg and B_2O_3, a low amount MgB_2 was observed in the final product. Additionally, the specific surface area and mean crystallite size of W_2B nanocrystals were measured as 18 m^2/g by N_2 absorption using Brunauer-Emmett-Teller (BET) method and about 13.61 nm via Scherrer formula respectively. The crystal structure of W_2B nanocrystals were found tetragonal and the lattice parameters a and c were found 5.568 Å and 4.744 Å respectively from the ICDD PDF Card of XRD graph at Figure 6. These results also match up with Coşkun et al. study [42].

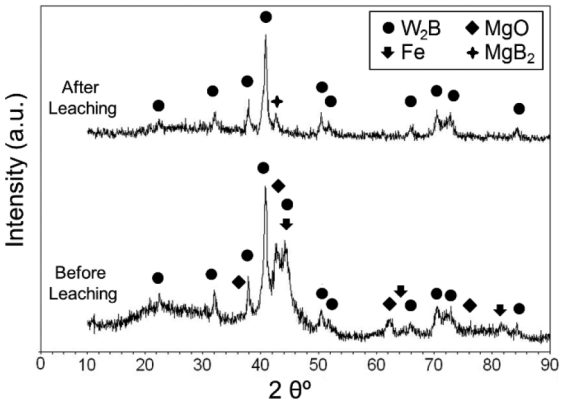

Figure 6. XRD pattern of W_2B nanocrystals

Figure 7 shows the SEM images of purified W_2B nanocrystals. As it can also be seen from this figure, particles were agglomerated again and mostly were in coaxial and spherical shape and morphology. The basic reason of the agglomeration was the because of cold welding of reactants due to mechanic energy released during the milling. The drying of purified particles under vacuum also contributed the agglomeration. It was determined from the SEM images that the agglomerates had a wide particle size distribution range under -2 µm.

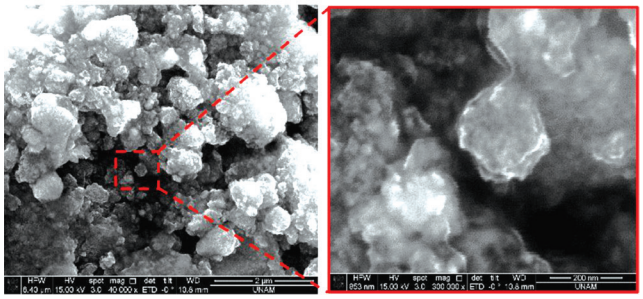

Figure 7. SEM images of W_2B nanocrystals after leaching

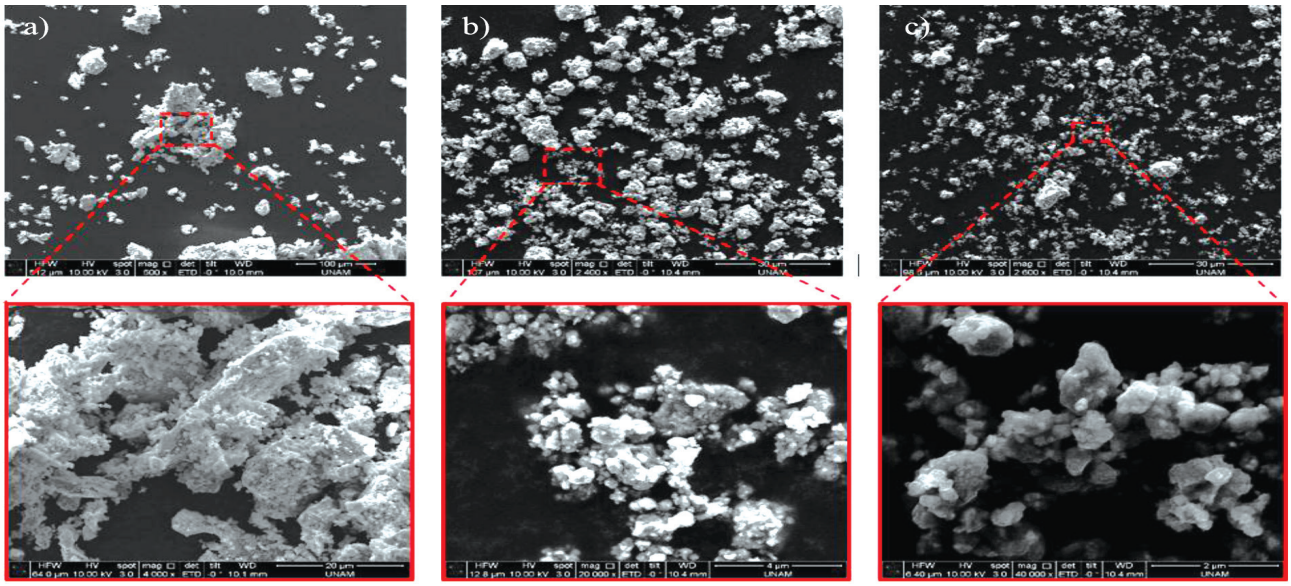

Figure 5. The SEM images of powders milled at 1h (a), 10 h (b) and 30 h (c)

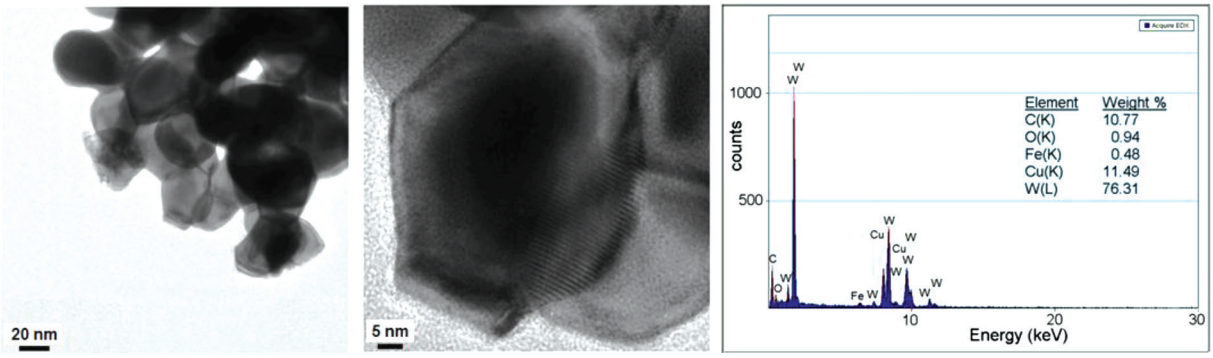

Figure 8. TEM images of W_2B nanocrystals after leaching

The TEM images of the W_2B nanocrystals after purification are shown in Figure 8. As seen clearly in this figure, intensive agglomeration was also observed with in various sizes due to the high energy ball milling. The single particle sizes were varied between about 40 and 80 nm. The EDS analysis of purified powders showed that W was the main phase, however low Cu and C peaks were observed due to used carbon coated copper TEM grid. In addition, B peaks were not observed in the EDS analysis because of its light atomic absorption characteristic.

4. Concluding remarks

Results of the experimental studies are summarized as follows;

- While W, W_2B, MgO, and Fe phases were observed with milling at 4:1:18 molar ratio, no W was observed at the end of 30 h milling performed at 4:2:18 molar ratio.
- W_2B nanocrystals were successfully obtained after the leaching with 2 M aqueous HCl solution at room temperature.
- The mean crystallite size of the nanocrystals was calculated as 13.61 nm.
- The specific surface area of nanocrystals was measured about 18 m^2/g by BET method.
- Intense agglomeration formations and nearly coaxial/spherical powder shape and morphology of W_2B nanocrystals were observed with SEM/TEM examinations.

Acknowledgment

The authors are very grateful to Eti Mine Works General Management for financial support and laboratory facilities usage.

References

[1] Li Q., Zhou D., Zheng W., Ma Y., Chen C., Global structural optimization of tungsten borides, Phys. Rev. Lett., 110 (13), 136403, 2013.

[2] Woods H. P., Jr. Wawner F. E., Fox G. B., Tungsten diboride: Preparation and structure, Science, 151 (3706), 75, 1966.

[3] Peshev P., Bliznakov G., Leyarovska L., On the preparation of some chromium, molybdenum and tungsten borides, J. Less Common Met., 13 (2), 241–247, 1967.

[4] Armas B., Trombe F., Chemical vapour deposition of molybdenum and tungsten borides by thermal decomposition of gaseous mixtures of halides on a solar “front chaud”, Solar Energy, 15 (1), 67–73, 1973.

[5] Tsirlin A. M., Khodov G. Ya., Zhigach A. F. Rabinovich R. A. Guzhov V. P., The electrical resistance of boron and of tungsten borides in boron filaments, J. Less Common Met., 67 (1), 137–141, 1979.

[6] Ellison E. G., Boone D. H., Some mechanical properties of boron-tungsten boride filaments, J. Less Common Met., 13 (1), 103–111, 1967.

[7] Itoh H., Matsudaira T., Naka S., Hamamoto H., Obayashi M., Formation process of tungsten borides by solid state reaction between tungsten and amorphous boron, J. Matter. Sci., 22 (8), 2811-2815, 1987.

[8] Radev D., Zahariev Z., Oxidation stability of B_4C-Me_xB_y, composite materials, J. Alloys Compd., 197 (1), 87–90, 1993.

[9] Otani S., Ishizawa Y., Preparation of WB_{2-x} single crystals by the floating zone method, J. Cryst. Growth, 154 (1), 81-84, 1995.

[10] Okada S., Kudou K., Lundström T., Preparations and some properties of W_2B, δ-WB and WB_2 crystals from high-temperature metal solutions, Jpn. J. Appl. Phys., 34 (1), 226, 1995.

[11] Gostishchev V. V., Boiko V. F., Pinegina N. D., Magnesiothermal synthesis of W–WB powders in ionic melts”, Theor. Found. Chem. Eng, 43 (4), 468–472, 2009.

[12]. Mohammadi R., Lech A. T., Xie M., Weaver B. E., Yeung M. T., Tolbert S. H., Kaner R. B., Tungsten tetraboride, an inexpensive superhard material, Proc. Nation. Acad. Sci., 108 (27), 10958–62, 2011.

[13] Yeh C. L., Wang H. J., Preparation of tungsten borides by combustion synthesis involving borothermic reduction of WO_3, Ceram. Int., 37 (7), 2597–2601, 2011.

[14] Yazici S., Derin B., Effects of process parameters on tungsten boride production from WO_3 by self-propagating high temperature synthesis, Matter. Sci. Eng. B, 178 (1), 89–93, 2013.

[15] Yazici S., Derin B., Production of tungsten boride from $CaWO_4$ by self-propagating high-temperature synthesis followed by HCl leaching, Int. J. Refract. Met. Hard Mater., 29 (1), 90–95, 2011.

[16] Khor K. A., Yu L. G., Sundararajan G., Formation of hard tungsten boride layer by spark plasma sintering boriding, Thin Solid Films, 478 (1–2), 232–237, 2005.

[17] Usta M., Ozbek I., Ipek M., Bindal C., Ucisik A. H., The characterization of borided pure tungsten, Surf. Coat. Technol., 194 (2–3), 330–334, 2005.

[18] Sugiyama S., Taimatsu H., Mechanical properties of WC–WB–W_2B composites prepared by reaction sintering of B_4C–W–WC powders, J. Eur. Ceram., Soc., 24 (5), 871–876, 2004.

[19] Dash T., Nayak B. B., Preparation of multi-phase composite of tungsten carbide, tungsten boride and carbon by arc plasma melting: characterization of melt-cast product, Ceram. Int., 42 (1), 445–459, 2016.

[20] Stadler S., Winarski R. P., MacLaren J. M., Ederer D. L., vanEk J., Moewes A., Electronic structures of the tungsten borides WB, W_2B and W_2B_5, J. Electron. Spectrosc. Relat. Phenom., 110–111, 75–86, 2000.

[21] Ip K., Khanna R., Norton D. P., Pearton S. J., Ren F., Kravchenko I., Kao C. J., Chi G. C., Thermal stability of W_2B and W_2B_5 contacts on ZnO, Appl. Surf. Sci., 252 (5), 1846–1853, 2005.

[22] Kayhan M., Hildebrandt E., Frotscher M., Senyshyn A., Hofmann K., Alff L., Albert B., Neutron diffraction and observation of superconductivity for tungsten borides, WB and W_2B_4 Solid State Sci., 14 (11–12), 1656–1659, 2012.

[23] Feng S. Q., Guo, F., Li J. Y., Wang Y. Q., Zhang L. M., Cheng X. L., Theoretical investigations of physical stability, electronic properties and hardness of transition-metal tungsten borides WB_x(x = 2.5, 3), Chem. Phys. Lett., 635, 205–209, 2015.

[24] Chong X. Y., Jiang Y. H., Zhou R., Feng J., Stability, chemical bonding behavior, elastic properties and lattice thermal conductivity of molybdenum and tungsten borides under hydrostatic pressure, Ceram. Int., 42 (2), 2117–2132, 2016.

[25] Iizumi K, Kudaka K, Maezawa D, Sasaki T., Mechanochemical synthesis of chromium borides, J. Ceram. Soc. Jpn., 107 (1245), 491–493, 1999.

[26] Welham N. J., Formation of nanometric TiB_2 from TiO_2, J. Am. Ceram. Soc., 83 (5), 1290–1292, 2000.

[27] Kudaka K., Iizumi K., Sasaki T., Okada S., Mechanochemical synthesis of MoB_2 and Mo_2B_5, J. Alloys Compd., 315 (1–2), 104–107, 2001.

[28] Kudaka K., Iizumi K., Izumi H., Sasaki T., Synthesis of titanium carbide and titanium diboride by mechanochemical displacement reaction, J. Mater. Sci. Lett., 20 (17), 1619–1622, 2001.

[29] Iizumi, K., Sekiya, C., Okadac, S., Kudou, K., Shishido, T., Mechanochemically assisted preparation of NbB_2 powder, J. Eur. Ceram. Soc., 26 (4–5), 635–638, 2006.

[30] Kim J. W., Shim J. H., Ahn J. P., Cho Y. W., Kim, J. H., Oh, K. H., "Mechanochemical synthesis and characterization of TiB_2 and VB_2 nanopowders, Mater. Lett., 62 (16), 2461–2464, 2008.

[31] Jiang X., Trunov M. A., Schoenitz M., Dave R. N., Dreizin E. L., Mechanical alloying and reactive milling in a high energy planetary mill, J. Alloys Compd., 478 (1–2), 246–251, 2009.

[32] Akgün B., Çamurlu H. E., Topkaya Y., Sevinç N., Mechanochemical and volume combustion synthesis of ZrB_2, Int. J. Refract. Met. Hard Mater., 29 (5), 601-607, 2011.

[33] Çamurlu H. E., Preparation of single phase molybdenum boride, J. Alloys Compd., 509 (17), 5431–5436, 2011.

[34] Balcı O., Ağaoğulları D., Duman İ., Öveçoğlu, M. L., Carbothermal production of ZrB_2–ZrO_2 ceramic powders from ZrO_2–B_2O_3/B system by high-energy ball milling and annealing assisted process, Ceram. Int., 38 (3), 2201-2207, 2012.

[35] Ağaoğulları D., Duman İ., Öveçoğlu M. L., Synthesis of LaB_6 powders from La_2O_3, B_2O_3 and Mg blends via a mechanochemical route, Ceram. Int., 38 (8), 6203–6214, 2012.

[36] Balcı Ö., Ağaoğulları D., Duman İ., Öveçoğlu M. L., Synthesis of CaB_6 powders via mechanochemical reaction of Ca/B_2O_3 blends, Powder Tech., 225, 136–142, 2012.

[37] Shao J., Xiao X., Fan X., Chen L., Zhu H., Yu S., Gong Z., et al., A low temperature mechanochemical synthesis and characterization of amorphous Ni–B ultrafine nanoparticles, Mater. Lett., 109, 203–206, 2013.

[38] Torabi O., Naghibi S., Golabgir M. H., Tajizadegan H., Jamshidi A., Mechanochemical synthesis of NbC–NbB_2 nanocomposite from the Mg/B_2O_3/Nb/C powder mixtures, Ceram. Int., 41 (4), 5362–5369, 2015.

[39] Jafari M., Tajizadegan H., Golabgir M. H., Chami A., Torabi O., Investigation on mechanochemical be-

havior of Al/Mg–B_2O_3–Nb system reactive mixtures to synthesize niobium diboride, Int. J. Refract. Met. Hard Mater., 50, 86-92, 2015.

[40] Torabi O., Ebrahimi-Kahrizsangi R., Golabgir M. H., Tajizadegan H., Jamshidi A., Reaction chemistry in the Mg–B_2O_3–MoO_3 system reactive mixtures, Int. J. Refract. Met. Hard Mater., 48, 102–107, 2015.

[41] C. Suryanarayana, Mechanical alloying and milling, Progress in Materials Science 46 1-184, 2001.

[42] Coşkun S., Öveçoğlu M. L., Room-temperature mechanochemical synthesis of W_2B_5 powders, Metall. Mater. Trans. A, 44 (4), 1805–1813, 2012.

[43] Nasiri-Tabrizi B., Ebrahimi-Kahrizsangi R., Bahrami-Karkevandi M., Effect of excess boron oxide on the formation of tungsten boride nanocomposites by mechanically induced self-sustaining reaction, Ceram. Int., 40 (9), 14235–14246, 2014.

[44] Bahrami-Karkevandi M., Ebrahimi-Kahrizsangi R., Nasiri-Tabrizi B., Formation and stability of tungsten boride nanocomposites in WO_3–B_2O_3–Mg ternary system: Mechanochemical effects, Int. J. Refract. Met. Hard Mater., 46, 117–124, 2014.